THREE-DIMENSIONAL SIMULATIONS OF ACCRETION DISK TORUS

Jung Lin (Doris) Lee
Draft version July 29, 2015

ABSTRACT

In this project, we investigate the dynamics of an accretion disk torus using the *Athena++* code. First, we examine the hydrodynamical behavior of the torus when perturbed by small non-axisymmetric modes and show that it gives rise to a global fluid instability known as the Papaloizou-Pringle Instability (PPI). We numerically simulate a slender torus and tracks its evolution into non-linear regimes. We experiment with various physical and numerical parameters to explore how it affects the torus simulation. By computing the mode amplitude in the linear regime before saturation, we can quantify the mode growth and compare the results with the analytical growth predicted by Goldreich et al. (1986) and Papaloizou and Pringle (1984).

Keywords: instabilities, hydrodynamics, methods:numerical, accretion:accretion disks

1. PAPALOIZOU PRINGLE INSTABILITY

An accretion tori can be realized for accretion disks at the Eddington luminosity where the hydrostatic equilibrium between radiation pressure and inward gravitational force. In high accretion rate or high energy systems, such as AGNs and qusars, radiation near the poles creates a hollow region near the central accreting object and results in the toroidal geometry. Papaloizou and Pringle (1984) considers uniform angular momentum, isentropic, locally-stable torus and after non-axisymmetric peturbation, global hydrodynamical instability arises, and growth rates on the order of dynamical timescales. The more general case of a nonuniform angular momentum torus is studied in **?** which also give rise to Kelvin-Helmholtz instabilities. Further studies conducts linear stability analysis of the case of the slender torus using a set of 2D height-averaged equations. These are applicable when examining lower order modes on the principal branch where the scaled azimuthal wavenumber $\beta < 0.59$, since the torus is in vertical hydrostatic equilibrium.

Linear stability analysis breaks down after Papaloizou-Pringle instability arises and the torus becomes nonlinear. 2D slender tori and 3D tori simulation is required to track the evolution of the torus in this nonlinear regime. Hawley found that the instability breaks the torus up into independent "planets" , which is a more stable configuration than the instabilities in the torus. Before the discovery of Magnetorotational Instability (MRI) (Balbus and Hawley (1991)), PPI provided a possible mechanism to generate turbulent viscosity for angular momentum transport in disks.

Other than the potential astrophysical application, the Papaloizou-Pringle instability is also of academic interest since there exist an analytical prediction for the mode growth Goldreich et al. (1986) , compared to results of numerical simulation. As noted in the case of a wide torus in Hawley (1991), numerical diffusion tends to suppress mode growth and stabilizes the torus. Therefore, this serves as a useful test case for the hydrodynamics scheme in *Athena++*. In this project, we reproduce the Hawley's 3D finite difference simulation in higher grid resolution and using more accurate hydrodynamics schemes in the new *Athena++* code.

1.1. *Numerical Methods*

To observe the effects of how the instability is affected by different parameters, we first conducted a series of low resolution 64^3 numerical experiments to qualitatively examine the behavior of the m=1 mode. In order to track its evolution, the simulations are carried out far into the nonlinear regime until the pressure maximum spiral into the innermost boundary. The results are summarized in Table 1. R_0/R_B, the ratio between the radius to pressure max and to inner boundary, defines the radial dynamic range of the grid. All the models uses an adiabatic equation of state where γ=5/3. t_{run} is denoted in units of orbits. The computation is carried out on Hopper, NERSC's Cray XE6 System and Edison, a Cray XC30 System.

1.1.1. *Initial Conditions*

As derived in Papaloizou and Pringle (1984), the initial conditions of the torus satisfies hydrostatic equilibrium.

$$-\frac{\nabla P}{\rho} - \nabla \psi_{pm} + \Omega^2 \tilde{\omega} \hat{\tilde{\omega}} = 0 \qquad (1)$$

where ψ_{pm} is the pseudo-Newtonian potential used in Blaes (1987)

$$\phi = \frac{-GM}{r - R_G} \qquad (2)$$

Here we approximate the Schwarzschild radius $R_G = 0$ since $R_G << R_0$ of the torus. The torus density that satisfies this condition is given by:

$$\rho(r,\theta) = \left[\frac{GM}{(n+1)AR_0} \left[\frac{R_0}{r} - \frac{1}{2} \left(\frac{R_0}{rsin\theta} \right)^2 - \frac{1}{2d} \right] \right]^n \qquad (3)$$

The cells in each r-θ slice of a torus is divided into a more refined 10×10 subgrid to better enforce the equilibrium condition in the initial condition. We ensured the stability of the torus by evolving it for over 30 orbits without perturbation and showed that there is no unstable modes.
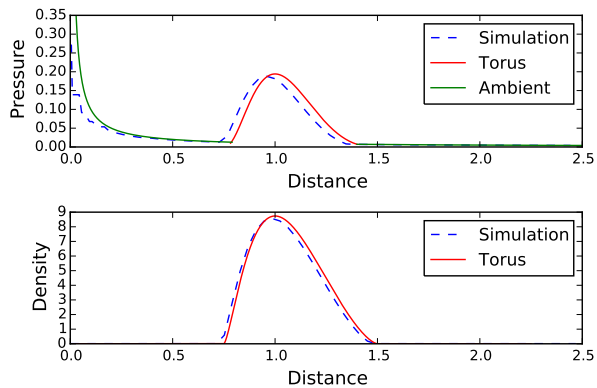
Figure 1. Density and Pressure profile in the initial condition taken from a $\theta = \pi/2$ slice.

The torus pressure is computely directly from the torus density, as given by the polytrope equation $P = A\rho^\gamma$. The constant A can be computed by setting $\rho_{max} = 1$, and therefore

$$A = \frac{(d-1)}{2d(n+1)}.$$

The gas density outside the torus (d_0) is chosen to be 10^{-4} and an ambient pressure profile of $P=d_0/r$ is setup in the initial condition. At the boundary of the torus, we compute the torus density compare it with d_0 and take the larger of the two to be the density. This smoothed out the discontinuities due to the piecewise definition of the physical quantities at the boundary of the torus, as shown in the radial profile in Fig 1 .

A pressure and density floor of either 10^{-8} and 10^{-6} is added in the simulations to prevent numerical artifacts of overflowed floating point that may affect our simulations. Extremely low density gas can appear outside of the torus, when much of the gas has flowed out of the computational domain. The pressure and density floor is several orders of magnitude less than the torus pressure and density, so it is physically negligible our consideration of the instability.

1.1.2. *Boundary Condition*

Global instabilities such as the PPI investigated here are often strongly dependent on the choice of boundary condition. Here we adopt the periodic boundary condition in the ϕ direction and outflow boundary condition in the outer radial boundary. Inner boundary condition was harder to chose since it can strongly affect the torus during stages of its nonlinear evolution as the torus spirals in towards the inner boundary. The selection of the R_0/R_B parameter on the inner boundary of the mesh isolates the central singularity and avoids regions of high gravitational potential as the high infall velocities limits the timesteps determined by the Courant Friedrichs Lewy (CFL) condition.

We tested out four combinations of the inner boundary condition by either setting outflowing V_R or $V_R=0$ and either a corotating boundary or $V_\theta=V_\phi=0$. The boundary conditions in Run B,D,E restricted the gas from spiraling inwards at later timesteps and results in high velocities that caused the simulation to terminate. Since excess free energy from shearing can drive other types of fluid instabilities, in order to distinctly observe PPI we need
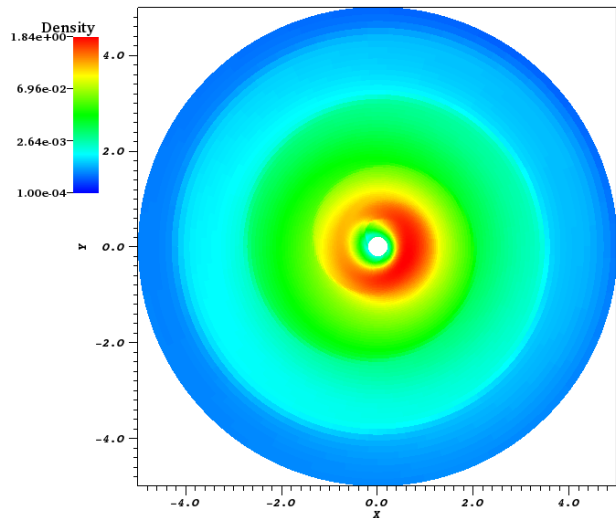
Figure 2. Z-slice of a 3D simulation of the torus showing spiral waves at the nonlinear regime (t=32 orbits).

to enforce the corotating boundary condition, so that the ghost zone moves with the boundary cells in the active computational domain. Along with setting the outflow radial velocity as zero as the gas hits the inner boundary, the resulting simulation alleviated the high velocities previously observed at the boundaries.

1.2. *Numerical Results*

1.2.1. *Effects of Distortion Parameter*

In Run F,G, we tried using two different distortion parameters that determines the shape of the torus. The value of d=1.1773 is derived from the r_{in} and r_{out} in the A2 slender torus model in Hawley (1991). For qualitative comparison, undistorted torus is smaller with a nearly-circular cross section as d→1. We find that the behavior of the two runs showed similar evolution, however, all the sequence of events in Run F occurred earlier in Run G than in Run F.

1.2.2. *Effects of Logarithmic Gridding*

Increasing the radial dynamic range using logarithmic gridding puts more gas into the computational domain so that the ambient conditions remains realistic for a longer period of time after the instability begins the drive the gas outside of the computational domain. Along with the proper boundary conditions as discussed in Sec 1.1.2, we no longer observe low density gas below the 10^{-6} density floor. We attempted at different multiplicative factors of logarithmic gridding in Run H, I, J and found that a factor of 1.03 is sufficient for covering the large radial domain. In Run I and J, the large logarithmic factor results in very fine grids near the inner boundary. Since there is high infall velocities due to the pseudo-Newtonian potential, the CFL condition strongly limits the timesteps of the simulation. In the future, Static Mesh Refinement (SMR) could be used to increase the resolution near the torus mid-plane region.

1.2.3. *Effects of Mode Initialization*

We describe two ways of initializing perturbation the simulation to trigger the PPI: random initialization and

Run	Grid	Δr	R_{in}, R_{out}	d	Perturbation	Inner B.C. (r, θ/ϕ)	t_{run} [orbits]	p/d floor
A	$256 \times 96 \times 256$	1.03	0.2,5.0	1.173	Random,1%	0,corotating	——	10^{-6}
B	$64 \times 64 \times 64$	1	0.2,2.5	1.173	Random, 1%	0,0	14.961	10^{-8}
C	$64 \times 64 \times 64$	1	0.2,2.5	1.173	Random, 1%	0,corotating	31.672	10^{-8}
D	$64 \times 64 \times 64$	1	0.2,2.5	1.173	Random, 1%	outflow,0	8.117	10^{-8}
E	$64 \times 64 \times 64$	1	0.2,2.5	1.173	Random, 1%	outflow,corotating	7.003	10^{-8}
F	$64 \times 64 \times 64$	1	0.2,2.5	1.125	Random, 0.1%	0,corotating	156.767	10^{-8}
G	$64 \times 64 \times 64$	1	0.2,2.5	1.173	Random, 0.1%	0,corotating	112.841	10^{-8}
H	$96 \times 64 \times 128$	1.03	0.2,5.0	1.173	Random, 1%	0,corotating	56.818	10^{-6}
I	$96 \times 64 \times 128$	1.05	0.2,5.0	1.173	Random, 1%	0,corotating	38.515	10^{-6}
J	$96 \times 64 \times 128$	1.09	0.2,5.0	1.173	Random, 1%	0,corotating	1.592	10^{-6}
K	$256 \times 96 \times 128$	1	0.2,2.5	1.173	Random,0.1%	0,corotating	24.048	10^{-8}
L	$96 \times 64 \times 128$	1.03	0.2,5.0	1.173	m=1, 0.1%	0,corotating	1.76	10^{-6}
M	$96 \times 64 \times 128$	1.03	0.2,5.0	1.173	m=1,0.001%	0,corotating	3.18	10^{-6}

Table 1
Selected parameters used in simulations.

eigenmode initialization. As done in Hawley (1991), for the random initialization, we added a unique, random number scaled by the amplitude to the gas pressure, which effectively adds enthalpy perturbation to each grid zone. For the eigenmode initialization, we added a perturbation of the form $A_0 sin(m\phi)$ in the ϕ-component of the momentum, where A_0 is the amplitude.

We begin by initializing with amplitude of 1% on the m=1 mode. However, the strong perturbation results in violent, nonlinear evolution within an orbital time. This makes the mode growth analysis difficult as the analytical mode growth derived by Goldreich et al. (1986) is based on a linear stability analysis, which does not give accurate prediction in the nonlinear regime after $t_{saturation}$. The 1% perturbation was acceptable when using the random initialization method because the amplitude of the perturbation does not directly translate into 1% amplitude for the m=1 mode growth. In the random initialization, any frequency mode can be possible, so the percentage of the actual amplitude that contributes to one specific mode amplitude is likely to be lower. Therefore, we decreased the amplitude to 0.001% for the m=1 eigenmode in Run M to conduct the analysis. In both types of initialization, we see strong m=1 mode growth and subsequent higher-order mode growth due to mode coupling.

1.3. *Mode Growth Analysis*

In order to quantify the results of the numerical simulation, we conduct the mode growth analysis and compare our result with the 3D numerical simulations done Hawley (1991) and the analytical growth rates given by Goldreich et al. (1986). To motivate the analysis of the eigenmodes, we first consider the physical mechanisms that give rise to PPI summarized in Narayan and Goodman (1989).

1.3.1. *Physical Mechanism*

Based on the torus boundaries on the z=0 plane in (Papaloizou and Pringle 1984),

$$\tilde{\omega}_{\pm} = \frac{\tilde{\omega_0}}{1 \mp \sqrt{1 - \frac{1}{d}}} \qquad (4)$$

where d is the distortion parameter, we obtained $(\tilde{\omega}_+, \tilde{\omega}_-) = (1.623, 0.723)$ for the case of a slender torus. Therefore, the scaled azimuthal wavenumber β is related

to the wave mode by $\beta = 0.45m$. The mode growth was computed by linear least square fit on the log-amplitude plot. Since we assume the form of the physical quantity to be $q(t) = q_0 e^{\frac{t}{\tau}}$ in the linear stability analysis, we can compute the mode growth by :

$$\tau = \frac{\Delta t}{log(\frac{x(t)}{x_0})} \qquad (5)$$

and verified that the values are similar to the previous numerical and analytical studies of mode growth in literature. For the m=1 modes, since the condition $\beta < 0.59$ is satisfied, it falls into the class of unstable modes known as the principle branch which has its corotation radius R_c at pressure maximum. Goldreich et al. (1986) showed that these can be reasonable approximated with a set of 2D height-integrated equations. The corotation radius (R_c) is the radius where the angular speed (Ω)is equal to the pattern speed(Ω_p), where the pattern speed is described $Re(\omega)/m$. R_c separates the inner region of the torus with negative action the outer region with positive action.

For the principal modes, the instability comes from the coupling between two traveling surface waves launched from the inner and outer edge of the torus. More generally, for higher-order modes, Narayan et al. (1987) describes amplification mechanism where the transmitted and reflected wave gets trapped near the evanescent region around R_c. With a satisfied phase condition, this amplification mechanism creates a feedback loop that reflects its own output back into the system, thus triggering the unstable mode growth seen in PPI. The principal mode is a special case of higher-order modes where the whole torus is the evanescent region, so the only waves that could interact and grow unstable are the traveling surface waves near $\tilde{\omega}_{\pm}$.

1.3.2. *Mode Growth Analysis*

The PPI give rise to unstable was modes that grows exponentially in time. We quantify the mode amplitudes by conducting a Fourier decomposition in the ϕ direction. The number of zones in the ϕ direction was chosen for this purpose to powers of two in order to speed up the Fast Fourier Transform (FFT) algorithm used to extract the modes.

We use a Python package h5py to read in the simulation data stored in HDF5 format per timestep. For
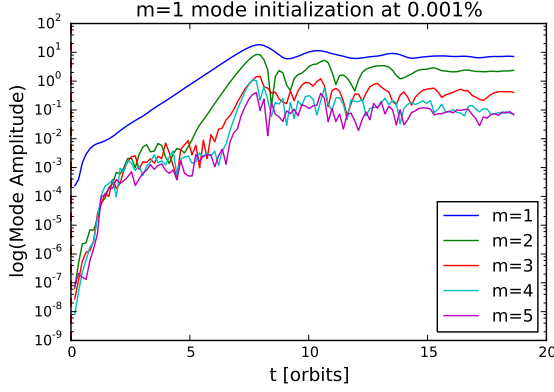
Figure 3. Mode growth of the m=1-5 initialized with m=1 mode at 0.001%.
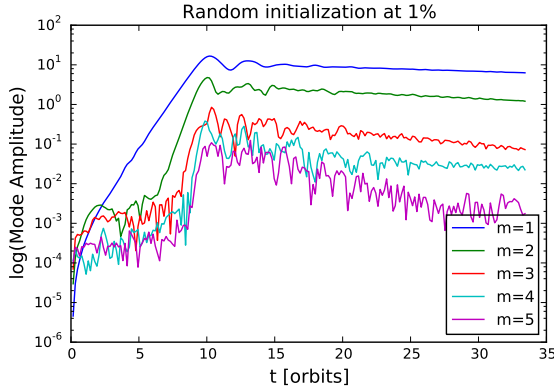
Figure 4. Mode growth of the m=1-5 with random initialization at 1%.

	Random Initialization		Eigenmode Initialization	
m=1	0.8679	0.855	0.2667	0.2621
m=2	0.4701	0.211	0.5505	0.5100
m=3	0.3756	0.254	0.6828	0.6820

Table 2
Left-flushed values are the mode growth in Run J, M respectively;
right-flushed values are mode growth in Hawley (1991).

every meshblock the datafile, we first compute the mass enclosed per cell in each $\Delta\phi$ slice by :

$$\frac{\text{M}_{\text{enclosed}}}{\Delta\phi} = \rho\Delta V_{\text{cell}} = \rho r^2 sin\theta \Delta r\Delta\theta \qquad (6)$$

$$D(\phi) = \sum_r \sum_\theta \rho\frac{\Delta V_{\text{cell}}}{\Delta\phi} \qquad (7)$$

Due to the z-ordering in the *Athena++'s* internal data structure, we use the the logical locations stored in each meshblock and sum over all the mass in a particular $r-\theta$ slice. This yields a 1D-array of length 128 containing the integrated mass per slice, $D(\phi)$. Then by Fourier decomposing the wave into 128 bins, we compute the magnitude by $|A| = \sqrt{\tilde{A} \cdot \tilde{A}^*}$. Fig. 2 and 3 shows the

mode growth of the m=1-5 modes. Table 2 summarizes the mode growth comparison with **?** for the random and eigenmode (m=1) initialization.

2. MAGNETOROTATIONAL INSTABILITY

2.1. *Numerical Methods*

2.1.1. *Initial Conditions*

To initialize an azimuthal field, we make use of the three degrees of freedom to set a convenient gauge that enables us to define $A_r = A_\phi = 0$ and $A_\phi = \frac{\rho^2}{\beta_0}$. We define initial conditions using the magnetic scalar potential at cell-corners and then compute $B(r,\theta)$ by $\nabla \times A$, rather than directly defining the initial condition using the face-centered magnetic fields to ensure the $\nabla \cdot \vec{B} = 0$ condition is satisfied in the discretized form. Using Stoke theorem to convert the $\vec{B}$ equation into an integral form,

$$\int \vec{B} \cdot d\vec{S} = \int A \cdot dl \qquad (8)$$

we can get the magnetic field by the simple discrete form:

$$\vec{B} = \frac{1}{\Delta S}[A_{\phi,+}l_+ + A_{\phi,-}l_-]. \qquad (9)$$

β_0 is a user-defined value for the plasma beta describing the ratio of gas-to-magnetic pressure. To maintain the initial hydrostatic equilibrium of the torus, we need to chose a β such that the initial azimuthal magnetic field is weak. Additionally, β also determines the scale height of the —- system.

In the case of PPI, there is a strict condition on the rotational velocity profile of constant angular momentum. This is not necessary for MRI to take place , in fact a Keplerian disk is okay.

REFERENCES

P. Goldreich, J. Goodman, and R. Narayan, MNRAS **221**, 339 (1986).
J. C. B. Papaloizou and J. E. Pringle, MNRAS **208**, 721 (1984).
S. A. Balbus and J. F. Hawley, ApJ **376**, 214 (1991).
J. F. Hawley, ApJ **381**, 496 (1991).
O. M. Blaes, MNRAS **227**, 975 (1987).
R. Narayan and J. Goodman, in *NATO Advanced Science Institutes (ASI) Series C*, edited by F. Meyer (1989), vol. 290 of *NATO Advanced Science Institutes (ASI) Series C*, p. 231.
R. Narayan, P. Goldreich, and J. Goodman, MNRAS **228**, 1 (1987).